Concrete Science and Engineering, Vol. 3, June 2001, pp 63-72

Early-age cracking resistance evaluation of concrete structures

H.-W. Song[1], H.-J. Cho[1], S.-S. Park[1], K.-J. Byun[1] and K. Maekawa[2]
(1) Department of Civil Engineering, Yonsei University, Seoul 120-749, Korea.
(2) Department of Civil Engineering, University of Tokyo, Tokyo 113, Japan.

ABSTRACT

Early-age defects in concrete such as thermal cracks and drying shrinkage cracks may limit the life span of concrete structures. For the construction of durable concrete structures, it is practical and rational to ensure durability performance by performing an examination of the cracking resistance of concrete structures at the design and construction planning stages and by ensuring cracking resistance during construction by modifying material design, construction plan or structural details. For that purpose, it is beneficial to find analytical techniques to examine the cracking resistance of concrete structures under construction conditions in advance. In this paper, a micro-level hydration model, which can consider different levels of hydration at different positions in the structure, and a moisture diffusion model along with a micropore structure development model are adopted and finite element heat transfer and moisture transport analysis for concrete wall structure is carried out. Then the process of stress development and crack occurrence in the concrete wall during the construction process is simulated. The effect of chloride ions in hydration, micropore structure formation and moisture transport for early-age concrete is also discussed and considered in the analysis.

1. INTRODUCTION

During the hydration process in early-age concrete, heat evolution and moisture diffusion occur simultaneously with the drying process. Due to volume changes caused by thermal expansion or contraction and high local tensile stress developed by shrinkage in a concrete structure, cracks may occur in the structure. Although, these induced cracks may not degrade structural safety immediately, they can affect the long-term durability performance of the concrete structure by permitting ingress of harmful external agents into the concrete more easily. Therefore, it is necessary to evaluate the crack resistance of concrete structures at an early age analytically in order to secure their long-term durability. If proper resistance of concrete to cracking cannot be obtained, re-examination will be carried out based on other material settings and mix proportions, and when the resistance is fulfilled in the examination, actual construction work can be advanced with the determined settings.

Although research on behavior of early-age concrete has been vigorous recently, attempts to link information known at micro level to practical one at macro level and further to predict behavior of concrete structure are relatively rare. Maekawa *et al.* [1] developed an analytical method which can predict structural behaviors of concrete under any specified environment and load through the unification of thermo-physics of materials and mechanics of structures. Van Breugel [2] also developed a numerical model which simulates hydration process, morphological features and material properties development in a combined manner. Borst and Boogaard [3], without considering micro level behavior, proposed a numerical strategy for fracture behavior of an early-age concrete structure.

In this paper, firstly we adopt analytical models for the hydration, micropore structure formation and moisture diffusion which were proposed for the modeling of early age concrete behaviors recently by Maekawa *et al.* [1] and verify the models and the subsequent shrinkage prediction with experimental data. Secondly, development models of mechanical properties such as strength and stiffness are proposed for the analysis of the crack resistance of early-age concrete structure. And then, through the unification of the models, finite element analysis is carried out to evaluate the crack resistance of a concrete wall structure with age during construction stages. The effect of chloride ions on the early-age behavior of con-

ISSN 1295-2826/01

crete manufactured with sea sand is clarified and is considered in the analysis.

2. MODELING OF EARLY AGE CONCRETE

2.1 Hydration heat model

The hydration heat of cement paste in concrete needs to be modeled as a phenomenon responsible for the creation of a hardened cement matrix and the source of temperature rise during hardening. It is an essential component for the evaluation of early-age cracking of concrete structures.

The hydration heat model used in this study is based on the so-called multi-component concept [4]. In view of the concept of a multi-component powder material, the effect of different types of cement can be rationally taken into account to predict the overall heat generation rate. The influence of variable moisture content or free water in the hydration is also taken into consideration in the concept. The chemical components of cement considered in this model are alite, belite, aluminate, ferrite and gypsum. Other powder materials like slag and fly ash can also be considered in the model as pseudo clinker components. The total heat generation rate of concrete H per unit volume is idealized as

$$H = C \,.\, H_c \qquad H_c = \sum p_i \,.\, H_i \tag{1}$$

where C is powder content per unit volume of concrete, H_c is specific heat generation rate of cement, H_i is specific heat generation rate of individual clinker component and p_i is the corresponding mass ratio in cement to total mass. The temperature dependant heat generation H_i of each clinker component is based on the modified Arrhenius' law of chemical reaction, where various coefficients represent the interaction among the constituents as follows

$$H_i = \beta_i \,.\, \gamma\, \xi\, \mu \,.\, s_i \,.\, H_{i,\,T_0}(Q_i) \,.\, \exp\left\{-\frac{E_i(Q_i)}{R}\cdot\left(\frac{1}{T}-\frac{1}{T_0}\right)\right\} \tag{2a}$$

$$Q_i = \int H_i dt \tag{2b}$$

Here, E_i is activation energy of i-th component reaction, $H_{i,\,T_0}$ is the referential heat generation rate when temperature is T_0 (= 293K) and R is gas constant. Additionally β_i represents the reduction of probability of the contact between unhydrated compound and free water, μ represents the effect of mineral composition of Portland cement, ξ represents the reduction of pozzolanic reaction due to shortage of calcium hydroxide, γ represents the retardation of cement and slag reaction caused by fly ash and organic admixture, and s_i represents the effects of fineness of reaction particles.

Finally, the temperature distribution and the degree of hydration of concrete can be obtained by applying the thermodynamic energy conservation to space and time domain of interest and using the hydration heat generation model as

$$\rho \,.\, c \,.\left(\frac{\partial T}{\partial t}\right) = div\,(k\nabla T) + H \tag{3}$$

where k is mean thermal conductivity of concrete, $\rho \,.\, c$ is heat capacity of concrete and H is concrete heat generation rate obtained from Equations (1) and (2).

For the verification of the model, measured temperature data from a mass concrete wall are compared with analysis results using this hydration heat model. Table 1 shows mix proportions of concrete. Finite element discretizations of the target wall structure cast on a hardened concrete footing are shown in Fig. 1 along with boundary conditions of the analysis.

The target structure is a massive concrete wall structure with 1.8m wall thickness and 3.5m height, which is restrained by a previously cast footing. Analysis results at two measuring points, in the center and on the surface of the wall, obtained from the hydration heat model are compared with experimental results as shown in Fig. 2. The comparison shows good agreement in the cooling phase except difference in the heating phase. This difference may be due to the comparison with different starting times for analyses and measurements.

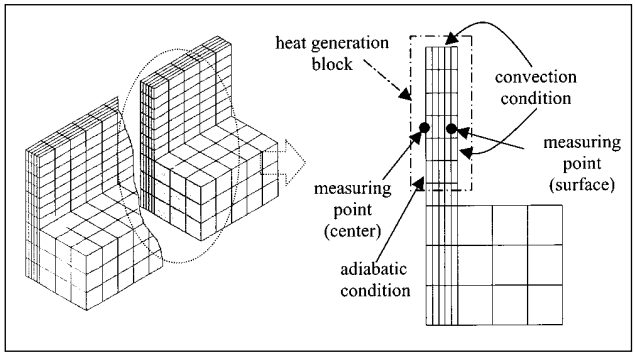

Fig. 1 – Finite element discretizations of target structure.

Table 1 – Mix proportions for hydration heat measurement

Cement type	W/C (%)	S/a %	Unit weight (kg/m³)				Admixtures (%)*		Mixing temperature
			C	W	S	G	WR	AE	
Type I	52	43	348	181	746	1060	0.3	0.007	20°C

C: cement, W: water, S: sand, G: gravel, a: aggregates (S + G), WR: water-reducing agent, AE: air-entraining agent.
*: percentage by cement content.

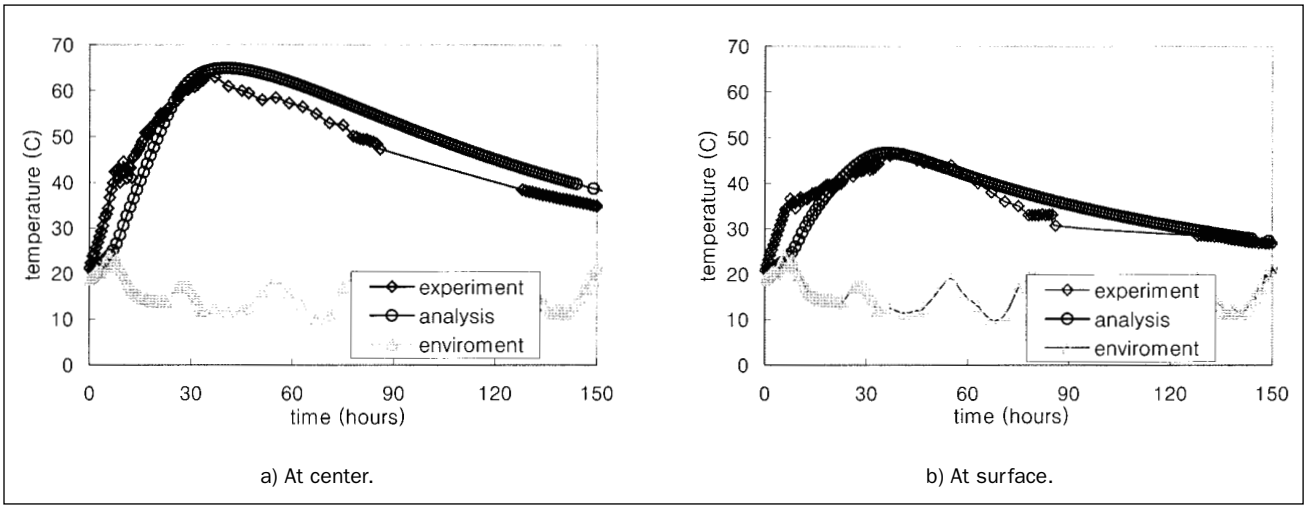

Fig. 2 – Temperature rises due to hydration.

2.2 Micropore structure formation model

Micropore characteristics of concrete have an important influence on its early-age properties. Especially, mass transport characteristics are directly related to micropore structure of cement paste matrix. Since long-term durability of concrete is primarily influenced by its mass transport characteristics, special attention has been given to the relationships of transport characteristics to the micropore structure.

In this study, a micropore structure formation model proposed by Chaube *et al.* [5] is adopted and verified. The micropore structure formation model assumes mono-sized particle dispersion and uses a particle expansion model based upon the degree of hydration. Furthermore, assuming a linear bulk porosity variation in the expanding cluster of a particle, important microstructural parameters such as surface area and bulk porosity distribution parameter, are computed with time. Finally, the model presents micropore distribution using a pore distribution function as

$$\phi(r) = \phi_{ir} + \phi_{gl} \cdot \{1 - \exp(-B_{gl} \cdot r)\} + \phi_{cp} \cdot \{1 - \exp(-B_{cp} \cdot r)\} \quad (4)$$

where r is radius of pore, and ϕ_{ir}, ϕ_{gl}, ϕ_{cp} are interlayer, gel and capillary porosity, respectively. B_{gl} and B_{cp} are capillary and gel porosity distribution parameter, which can be obtained from the relationship between surface areas and relevant porosities of the capillary and gel.

The predicted micropore structure of concrete can be used as a basis for a moisture transport model and strength and stiffness development prediction. Pore size and distribution of concrete computed by using the model are examined by mercury intrusion porosimeter (MIP) for verification of the proposed model. Fig. 3 shows the experimentally-obtained incremental volume of pores according to different pore radii at 3 days and 28 days, respectively. Fig. 4 shows a porosity comparison of analysis results and experimental results. It shows that the model predicts well the tendency in pore size distribution according to different ages except some difference in the cumulative porosity.

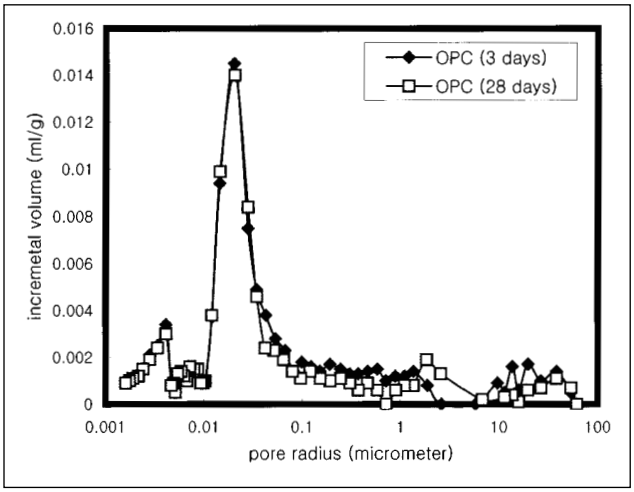

Fig. 3 – Pore distribution by MIP.

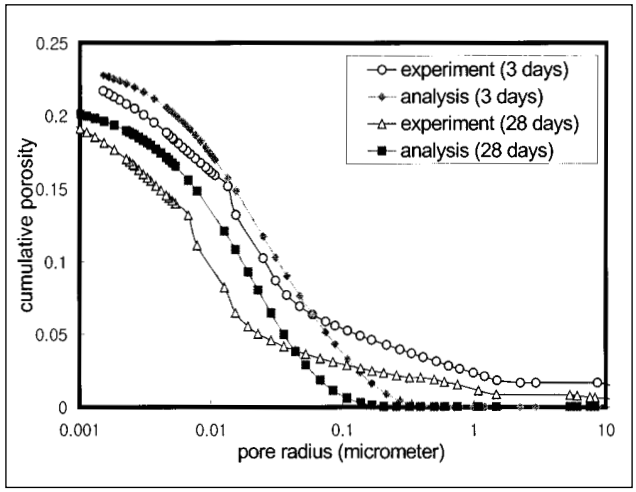

Fig. 4 – Porosity.

2.3 Moisture transport model and shrinkage prediction

The process of moisture transport in a porous medium can be distinguished by five major steps [6]. The first step is adsorption of water molecules to a solid pore surface. Subsequent to this, an unimpeded flux of vapor takes place where the vapor behaves like an ideal gas. Gradually, as the vapor pressure increases due to the vapor flux in the pore, condensation occurs at the neck of the pore. With increase in the thickness of the surface adsorbed water, a flow in thin liquid films may occur. Eventually, there is a transition to the final stage where the vapor pressure increases and condensation occurs within the pore and saturated flow begins in the porous system.

For solution of the mass transport problem, the total gas pressure in the porous media is assumed to be constant and equal to the atmospheric pressure. Compared to the liquid mass, the total mass of vapor is small enough to be ignored. The velocity of the liquid phase movement is very small and no acceleration of the liquid phase takes place as it moves in the porous media. By considering the quasi-equilibrium conditions of the movement and introducing the additional sink term of moisture content change in a control volume, a moisture transport model can be represented as

$$\alpha_p \cdot \frac{\partial P}{\partial t} - div\,(k \cdot \nabla P) + Q_p = 0 \tag{5}$$

where α_p is moisture capacity obtained from isotherms of moisture retention, k is coefficient of transport, and P is the equivalent liquid pore pressure. The loss term Q_p is the rate of internal moisture loss due to hydration and related effects.

By adopting the capillary tension theory to describe the mechanism of drying shrinkage in concrete, the pressure difference between the liquid phase and the gas phase is assumed as the cause of the shrinkage deformation. Under equilibrium conditions, the liquid moisture would generally be under equilibrium with the vapor phase surrounding the completely filled pores. For such a system, a small change in the vapor pressure would cause a corresponding change in the liquid pressure. The pressure difference due to capillarity across the liquid-vapor interface can be obtained as follows

$$\Delta P_c = P_G - P_L = \frac{\rho \cdot R \cdot T}{M} \cdot \ln h \tag{6}$$

where ΔP_c is pressure difference due to capillarity, P_G is gas pressure, P_L is liquid pressure, R is universal gas constant, T is absolute temperature of the vapor-liquid system, M is molecular mass of the water, and h is relative humidity, *i.e.* the ratio of the vapor pressure to the saturated vapor pressure.

The pressure difference between the liquid and vapor phase would be balanced by the curved vapor-liquid interface formed in numerous pores of the structure. Thus, this pressure difference can be explained by the effect of the surface tension of liquid water. If the interface is assumed to be a part of an ideal spherical surface, the following Laplace's equation can be obtained:

$$\Delta P_c = P_G - P_L = \frac{2 \cdot \gamma}{r_s} \tag{7}$$

where γ is the surface tension of liquid water and r_s is a pore radius at which the interface is created. It is also assumed that tensile stress due to the pressure difference applied on the pore walls causes the shrinkage of concrete [7, 8]. Since autogenous shrinkage and drying shrinkage are the same in terms of decrease of humidity in the hardened cement body, the tensile stress σ_s due to the decrease in the relative humidity of the pores is assumed as the cause of both the autogenous and drying shrinkage strains ε_{sh}, which can be written as

$$\sigma_s = \frac{2 \cdot \gamma}{r_s} = \frac{\rho \cdot R \cdot T}{M \cdot \ln h} \tag{8}$$

$$\varepsilon_{sh} = A_s \cdot \frac{\sigma_s}{E_s} \tag{9}$$

where A_s is area factor and E_s is elastic modulus on capillary tension. Note that the E_s is usually 2~4 times smaller than instantaneous elastic modulus of hardened concrete depending on rate of drying and microstructural conditions [7] and is defined only at the stage of the moisture transport.

In order to verify the model, an analysis is carried out and then analytical results are compared with the test results. In the test, shrinkage behaviors such as time-dependent weight and length changes are measured for two specimens having different water-cement ratios. Mix proportions and test conditions for the specimens are shown in Table 2. Dewatering amount is obtained by measuring weight loss of specimens and shrinkage strain is measured by using an embedded strain gage with a length of 60 mm. Comparisons of the dewatering amount and the shrinkage strain are shown in Figs. 5 and 6, respectively. These comparisons show that analytical results agree well with experimental ones.

Table 2 – Mix proportions and test conditions for dewater and shrinkage measurement								
Mix	W/C (%)	S/a (%)	Unit weight (kg/m³)				Specimen shape and size (cm)	Drying condition
			C	W	S	G		
1	45	44.5	406	183	805	1004	Cubic 10 × 10 × 10 – dewatering	60 % RH, 20°C
2	55	46.5	333	183	869	1000	Prims 10 × 10 × 40 – shrinkage	after 1 day

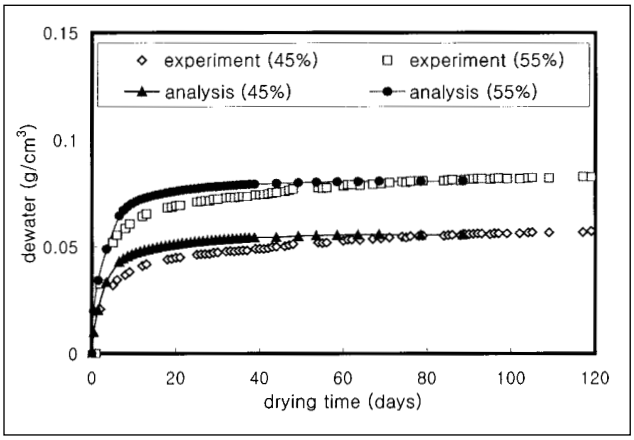

Fig. 5 – Dewatering amount.

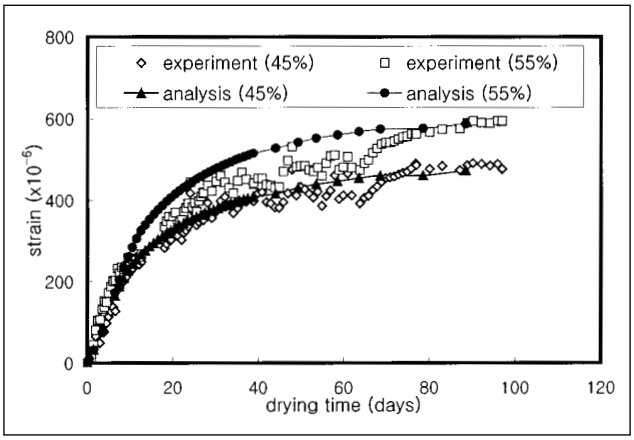

Fig. 6 – Shrinkage strain.

2.4 Mechanical properties development model

Since the stress due to volume change of early-age concrete depends on developed stiffness and the crack resistance due to this stress depends on developed strength, an accurate estimation of the mechanical properties such as strength and stiffness, *i.e.*, compressive strength and elastic modulus, of early-age concrete is necessary for the evaluation of the early-age cracking resistance of concrete structures.

The mechanical properties obtained from standard specimen tests, which do not reproduce the actual temperature hysteresis of concrete structure itself, cannot represent the mechanical properties of the structure. In the design process, experimental estimation of the development of mechanical properties with age at all positions in a concrete structure is almost impossible, so an analytical model which can consider the effects of both temperature and time is necessary. This study proposes an early-age compressive strength development model based on the so-called maturity concept. The model depends on the hydration degree and takes into account the effects of time, temperature and porosity. For the elastic modulus of early-age concrete, a micro-mechanics based evaluation model considering composite material behavior is also proposed.

The compressive strength of concrete depends upon, not only the intrinsic proportions of its mixture, but also its age and temperature at a position where it hardens. During the later 1940s and early 1950s, the maturity concept was proposed to account for the combined effects of time and temperature on strength gain. While maturity expressed as a product of time and temperature is simple enough, it is not directly linked with strength. Rastrup [9] proposed a concept of "equivalent age", which is defined as the time that concrete would have to be cured at a reference temperature to achieve the same maturity as the concrete under actual curing history. Chanvillard and D'Aloia [10] suggested a strength estimation model using Arrhenius' law based on this concept. By modifying their strength estimation model, a strength development model is proposed as Equation (10) by utilizing the hydration degree obtained from the aforementioned multi-component hydration heat model. In order to consider the effect of porosity, an additional parameter $\overline{\gamma_c}$ (which is obtained from the micropore structure formation model) is introduced in the equation.

$$S_c = \overline{\alpha}_c \cdot \overline{\gamma}_c \cdot S_{c28,\,T_{20}} \cdot [1 - k\,(T - 20)] \qquad (10)$$

where S_c is developed strength, $S_{c28,\,T_{20}}$ is 28-day strength obtained under referential isothermal curing temperature 20°C, T is curing temperature (°C), k is constant (= 0.01, for normal case), $\overline{\alpha_c}$ is normalized hydration degree, $\overline{\gamma_c}$ (= $e^{-n\,\cdot\,(1-\overline{p})}$) is porosity parameter, $\overline{p}$ is normalized porosity and n is material constant.

Since concrete is a composite of coarse aggregates, fine aggregates, hydrated cement pastes (HCP) and interfacial transition zones (ITZ) which have different material properties and volume fractions, it is difficult to evaluate its elastic modulus analytically [11]. In this study, a micromechanics-based scheme [12] is proposed to obtain the elastic modulus of early-age concrete by utilizing information on the degree of hydration.

Through the averaging of a two-phase triple-layered inclusion model using the self-consistent method [13], the following simultaneous Equation (11) is obtained in terms of effective bulk modulus $\overline{K_r}$ and shear modulus μ_r at a referential time (*e.g.* 28 days) of concrete. Then, the effective elastic modulus can be obtained by solving the Equation (11) simultaneously.

$$f_1\left\{\frac{\overline{K_r}}{\overline{K_r}-K_r^1}-\overline{s_1}\right\}^{-1}+f_2\left\{\frac{\overline{K_r}}{\overline{K_r}-K_r^2}-\overline{s_1}\right\}^{-1}+f_M\left\{\frac{\overline{K_r}}{\overline{K_r}-K_r^M}-\overline{s_1}\right\}^{-1}+f_\Gamma\left\{\frac{\overline{K_r}}{\overline{K_r}-K_r^\Gamma}-\overline{s_1}\right\}^{-1}=0 \quad (11a)$$

$$f_1\left\{\frac{\overline{\mu_r}}{\overline{\mu_r}-\mu_r^1}-\overline{s_1}\right\}^{-1}+f_2\left\{\frac{\overline{\mu_r}}{\overline{\mu_r}-\mu_r^2}-\overline{s_1}\right\}^{-1}+f_M\left\{\frac{\overline{\mu_r}}{\overline{\mu_r}-\mu_r^M}-\overline{s_1}\right\}^{-1}+f_\Gamma\left\{\frac{\overline{\mu_r}}{\overline{\mu_r}-\mu_r^\Gamma}-\overline{s_1}\right\}^{-1}=0 \quad (11b)$$

where f is volume fraction, and K_r and μ_r are bulk and shear modulus at referential time, respectively. The indices 1, 2, M and Γ represent coarse aggregate, fine aggregate, hydrated cement paste and interfacial transition zone, respectively. The coefficients s_1, s_2 are obtained from the decomposition of Eshelby's tensor [13]. In order to take into account the influence of the maximum aggregate size and aggregate gradation on the volume fraction of ITZ, the method proposed by Li *et al.* [14] is adopted. Then, elastic modulus $\overline{E_c}$ can be obtained by introducing the hydration degree $\overline{\alpha_c}$ obtained from the multi-component hydration heat model and porosity parameter $\overline{\gamma_c}$ obtained from the micropore structure formation model, respectively as

$$\overline{E_c}=\overline{\alpha_c}\cdot\overline{\gamma_f}\cdot\frac{9\cdot\overline{K_r}\cdot\overline{\mu_r}}{3\cdot\overline{K_r}+\overline{\mu_r}} \quad (12)$$

In order to verify the models, results of compressive strength tests by Kim *et al.* [15] are compared with analysis results using the model. Kim *et al.* investigated the effects of varying temperatures occurring at different ages on the concrete strength.

For this purpose, they considered four different points of curing time with an individual interval of 24 hours: 0th~1st, 1st~2nd, 2nd~3rd, and 6th~7th days of selective curing interval from the start of curing. High curing temperature of 40°C is applied for these four intervals, whereas remaining days are cured at the reference curing temperature of 20°C. As shown in Table 3, the concrete is proportioned using different water to cement ratio of 0.55 for normal strength concrete (NSC) and 0.35 for high strength concrete (HSC) to obtain concretes with different strengths. Fig. 7 shows FE modeling along with boundary conditions of a standard specimen for the analysis.

Table 3 – Mix proportions for compressive strength measurement

Mix	W/C (%)	S/a (%)	Unit weight (kg/m³)				Admixtures (%)		Initial temperature
			C	W	S	G	SP	AE	
NSC	55	47	335	185	835	959	–	0.2	20 ± 2°C
HSC	35	45	495	175	759	940	1.0	0.2	

NSC: Normal Strength Concrete, HSC: High Strength Concrete, SP: superplasticizer.

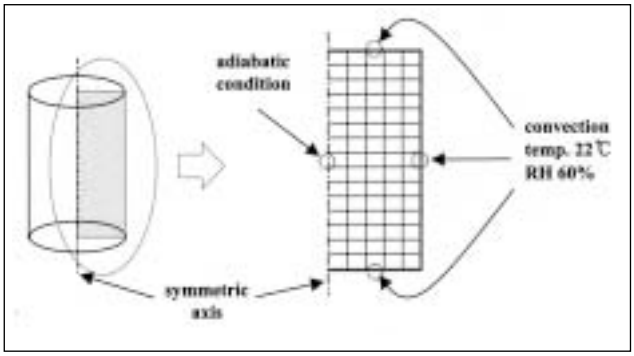

Fig. 7 – FE model of standard specimen.

As shown in Table 4, analytical results are in good agreement with experimental data for concrete under various curing conditions. Fig. 8 shows comparison of compressive strength development at concrete between isothermally cured during 0th~28th days at 20°C (N20 (0,28), H20 (0,28)) and selectively cured at 40°C during 0th~1st day (N40 (0,1), H40 (0,1)).

Table 4 – Comparison of compressive strength at different curing conditions

W/C	Curing method	Compressive strength (MPa)					
		1 day	2 days	3 days	7 days	14 days	28 days
0.55	N20 (0,28)	7.74 (6.96)	13.5 (12.1)	18.1 (16.4)	27.5 (25.1)	32.5 (31.7)	35.8 (35.9)
	N40 (0,1)	13.1 (16.7)	18.4 (20.9)	20.2 (22.8)	25.2 (26.0)	28.6 (29.1)	31.3 (31.1)
	N40 (1,2)	–	17.1 (18.3)	21.1 (22.4)	26.8 (27.4)	30.5 (30.3)	33.4 (31.9)
	N40 (2,3)	–	–	20.6 (20.7)	27.5 (26.9)	31.2 (30.5)	34.1 (32.9)
	N40 (6,7)	–	–	–	28.1 (25.8)	32.4 (31.6)	35.4 (33.7)
0.35	H20 (0,28)	16.3 (12.2)	26.6 (24.4)	31.1 (30.9)	38.2 (39.6)	43.9 (45.5)	50.0 (49.6)
	H40 (0,1)	29.4 (27.6)	32.0 (32.3)	33.2 (33.6)	36.9 (37.9)	41.4 (42.8)	46.5 (46.3)
	H40 (1,2)	–	31.9 (33.2)	34.7 (35.3)	39.2 (40.7)	44.1 (43.9)	49.6 (48.2)
	H40 (2,3)	–	–	34.3 (37.8)	39.8 (40.2)	44.7 (45.5)	50.3 (50.3)
	H40 (6,7)	–	–	–	39.7 (40.9)	45.1 (45.3)	50.8 (51.3)

– Values in parentheses are compressive strength obtained from tests.

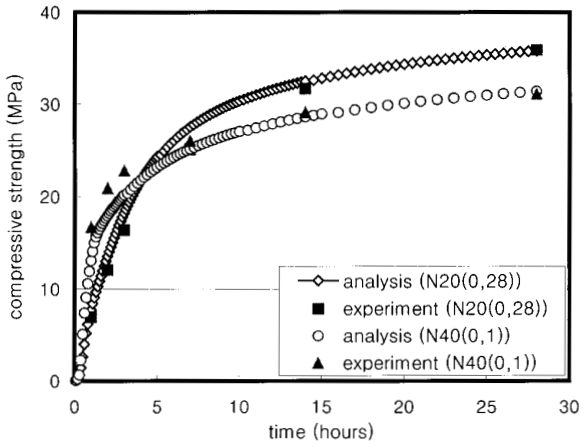

a) Normal strength concrete.

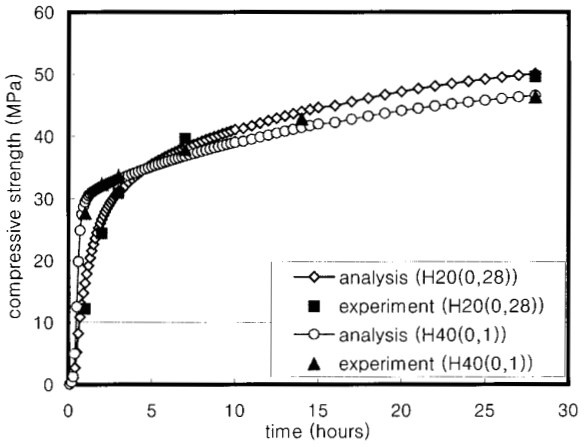

b) High strength concrete.

Fig. 8 – Compressive strength developments.

3. EFFECT OF CHLORIDE IONS IN EARLY-AGE BEHAVIOR

With increased use of sea sand due to depletion of inland sand, research on the characteristics of concrete using sea sand has been active. However, studies on the early-age behavior of the concrete are still lacking compared to studies on long-term durability problems such as steel corrosion inside the concrete. Especially, the effect of $CaCl_2$ as an accelerator in the concrete is mainly studied, but the effect of NaCl which is a main component of salts in sea sand is rarely studied. In this paper, the effect of NaCl on the early-age behavior of concrete is studied.

3.1 Effect of chloride ions to hydration

Free chloride ions in concrete decrease the pH of the solution and then accelerate hydration. Recently, Brown *et al.* [14] studied the characteristics of hydration of C_3S in many kinds of salts solution with the same anion molarity by using a conduction calorie-meter and solution phase analysis. They found that $Ca(OH)_2$ was generated actively in solution with hydroxyl ions (OH^-) as the concentration of Ca^{2+} ions increased. This loss of the OH^- decreases the pH of the solution, and then the hydration reaction rate increases. They also observed that acceleration of hydration occurs with the decrease in concentration of calcium ions at an early age. In the case of sodium chloride, however, the reduced concentration of calcium ion was not found by water solution analysis.

In this study, in order to analyze the effects of NaCl, which occupies 80% of salts in sea sand on hydration, adi-

abatic temperature raise tests are carried out. In the tests, characteristics of hydration heat corresponding to different chloride ion contents (0.3 kg/m³ and 0.6 kg/m³, respectively) are obtained. Table 5 shows mix proportions used in the tests. An adiabatic temperature rise curve and a hydration heat release rate curve are shown in Figs. 9 and 10, respectively. This shows that there is almost no difference in characteristics of hydration heat when using chloride ions less than an amount of 0.6 kg/m³.

Table 5 – Mix proportions for measurement of effect of chloride ions to hydration

Cement type	W/C (%)	S/a (%)	Unit weight (kg/m³)				Admixtures (ml)		Mixing temperature
			C	W	S	G	WR	AE	
Type	35	42	523	183	719	993	2514.0	17.3	20°C

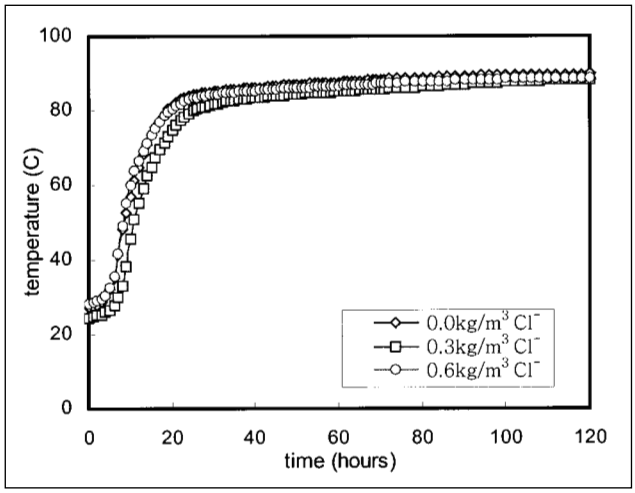

Fig. 9 – Adiabatic temperature raise curve for different chloride ion contents.

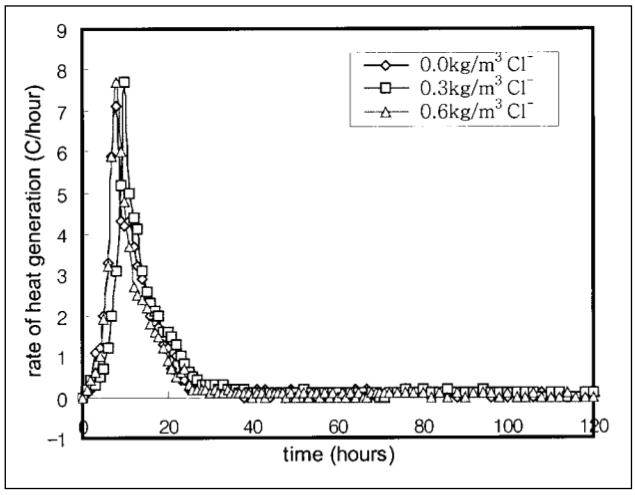

Fig. 10 – Hydration heat generation rate for different chloride ion contents.

3.2 Effect of chloride Ions to shrinkage

In this study, the shrinkage characteristics of concrete containing a certain amount of chloride ions are clarified by experiment and then these are used to modify the shrinkage prediction equation. Four different amounts of chloride ions (0, 0.07, 0.6 and 1.2% of unit cement weight, respectively) are added to the mix proportions of concrete with two different water-cement ratios as previously shown in Table 2. A day after casting, the molds are removed. The curing condition is a temperature of 20° ± 5°C, and humidity of 60 ± 5%. Shrinkage measurement of cylinder specimens (15 × 30) is obtained using an embedded strain gage with a length of 60 mm. Increased shrinkage strain with increases of chloride ions quantities is obtained from experiment. Even it is not clearly verified whether the increased shrinkage strain is due to the increased chloride ions quantities, we simply assume and modify Equation (9) as a function of the concentration of chloride C_{cl}. Then, Equation (9) becomes

$$\varepsilon_{sh} = \frac{\sigma_s}{E_s}\,(a + b\,.\,C_{cl}{}^{c}) \qquad (13)$$

where a, b and c are experimental constants, respectively, and E_s is elastic modulus. The proposed shrinkage model is verified through comparison with experimental results. Fig. 11 shows the comparison of shrinkage strains for different water-cement ratios.

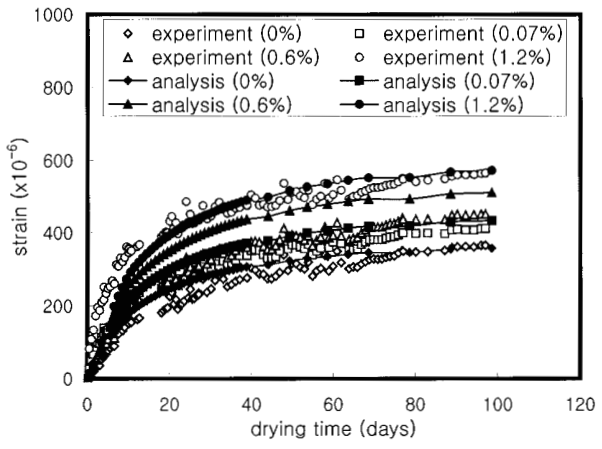

a) W/C = 45%.

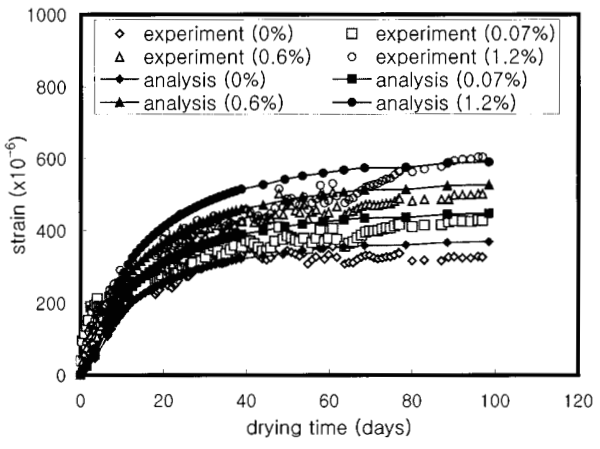

b) W/C = 55%.

Fig. 11 – Shrinkage strains.

4. CRACK RESISTANCE ANALYSIS OF EARLY-AGE CONCRETE

Cracks occurring in early-age concrete may affect the durability performance of concrete structures. Although it is not clear how much these defects influence the durability performance, the performance can be secured in a sense if cracks are prevented in the construction stage or if the crack width is limited. Therefore, a proper cracking resistance evaluation at the construction stage is necessary during construction planning, where construction methods along with material selections can be easily re-examined according to the results of the evaluation.

In this paper, an analysis to evaluate the cracking resistance of a concrete structure at an early age is carried out through unification of the aforementioned models into a finite element program. For this analysis, unconfined thermal and shrinkage deformation are initially obtained. Then, a stress analysis is carried out by applying the initial analysis results to a target concrete structure with the restraint conditions of the structure. Finally, crack occurrence for the concrete structure is judged by comparing stress induced and strength developed. Fig. 12 shows a schematic view of the unified FE analysis. Table 6 shows the material properties used in the stress analysis. In this analysis, assuming the effect of creep is relatively small, the concrete is assumed to be an elastic body but further research will contain the relaxation effect at early-age.

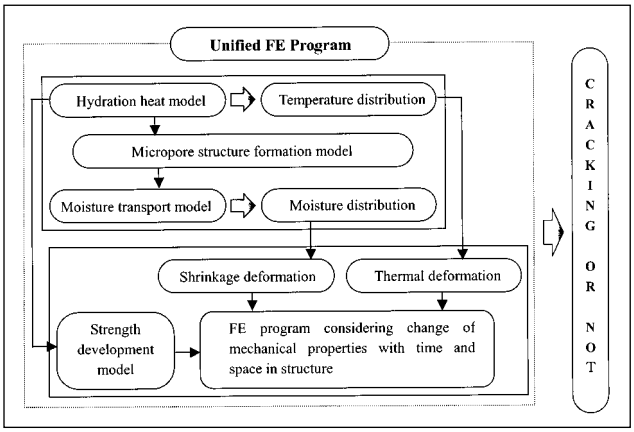

Fig. 12 – Schematic view of unified FE analysis for cracking resistance.

Table 6 – Material properties for stress analysis	
Thermal expansion coefficient (/K)	10×10^{-6}
Poisson's ratio	0.18
Tensile strength (MPa)	$f_t(t) = 1.4\sqrt{f_c'(t)}$

* $f_c'(t)$ is compressive strength with age.

The target structure for the analysis is a newly cast mass concrete wall structure on a previously constructed and hardened concrete foundation as shown in Fig. 13. The wall has 1.2 m thickness, 4.0 m height, and 15.0 m length. The wall has a high probability of cracking due to hydration heat and drying shrinkage. Initial conditions for analysis are 20°C for heat analysis and RH 100% until 5 days for moisture analysis. Environmental conditions are 20°C and RH 60% for heat and moisture analysis, respectively. As shown in Fig. 13, the advantage of the two planes of symmetry is considered in the FE discretization.

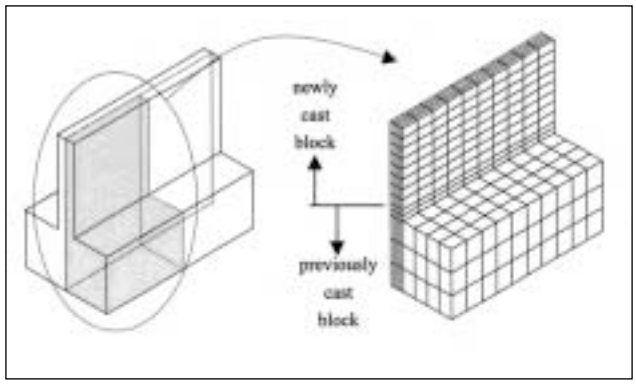

Fig. 13 – FE discretization of target structure.

The analysis of crack resistance is carried out for two different cases: one for concrete containing no chloride ions and the other for concrete containing 0.07% chloride ions in the weight of cement because of use of sea sand. The mix proportions used are Mix 1 from Table 2. Dots on the wall section in Fig. 14 are checking points for crack occurrence. Fig. 15 shows analytical results of temperature variations with age at each point.

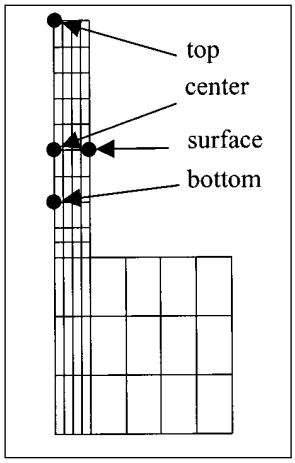

Fig. 14 – Checking points for crack occurrence.

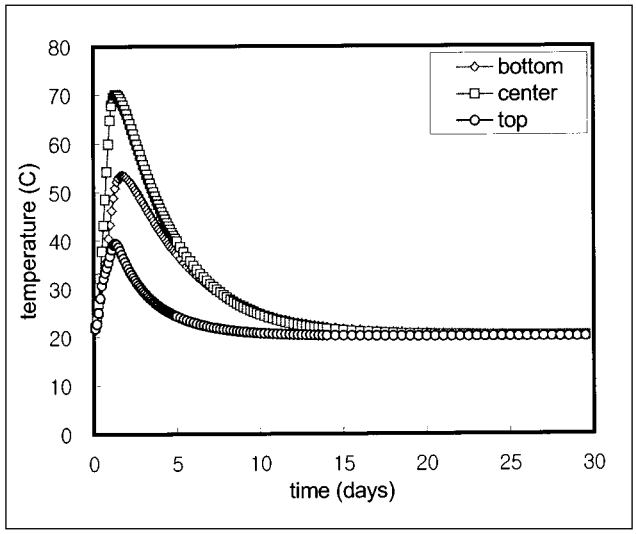

Fig. 15 – Temperature variations with age.

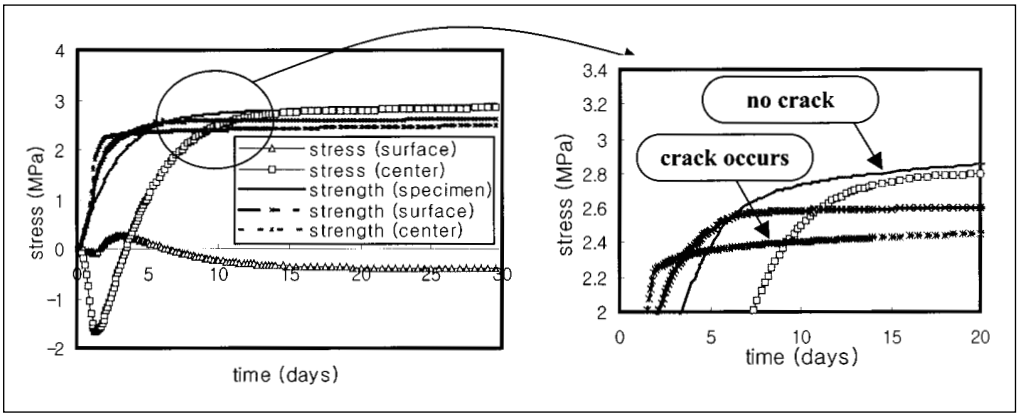

Fig. 16 – Crack assessment with induced stress and developed strength.

Since every point in the target structure experiences different temperature histories, developed strengths at each location of the structure differ from those of the specimen. Generally, concrete cured at high temperature at an early age attains higher early-age strength but eventually attains lower later-age strength than the standard specimen cured at a referential temperature, as shown in Fig. 8. Fig. 16 shows a comparison between induced stresses of the wall due to hydration heat and developed strengths of the specimen and the wall. The strength development at the center is faster than that at the surface and that of the specimen at a very early age, but strength reduction occurs remarkably at the center with age. As shown in Fig. 16, if the strength development of the specimen is used for a reference to assess the crack occurrence, no crack is judged to have occurred at the center of the wall. However, if the strength development at the center of the structure is used for the reference by considering actual temperature history, cracks occur about 9 days after casting. Since conventional analysis schemes seldom consider this temperature-dependent strength development, the proposed analysis scheme is more rational and can be used for crack resistance evaluation of early-age concrete more accurately.

Fig. 17 shows stress variations with age for cases of use of inland sand and sea sand, *i.e.*, without and with chloride content, respectively. Since the use of sea sand accelerates strength development and increases shrinkage strain at an early age, induced stress for concrete using sea sand becomes slightly larger than that for concrete using inland sand.

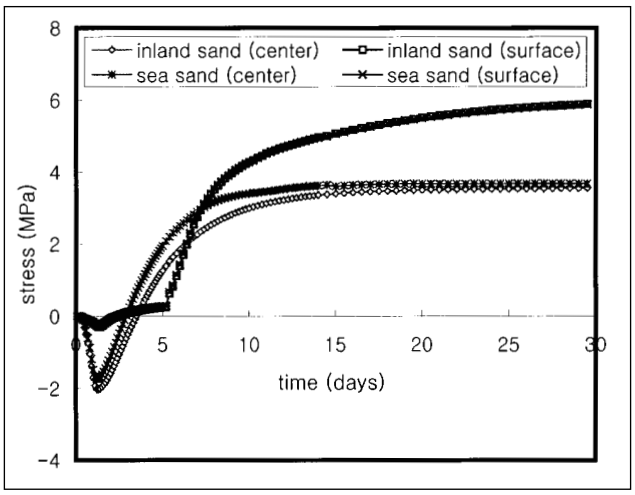

Fig. 17 – Stress variations with age.

5. SUMMARY AND CONCLUSION

The following conclusions can be drawn from this study.

1) Characteristics of heat conduction in concrete at an early age are simulated using a multi-component hydration heat model which can consider the temperature-dependent hydration reaction and change of mix proportions. The proposed model is verified by in-situ temperature data.

2) The Pore size distribution of a cement paste matrix is obtained with a micropore structure formation model which quantifies pore distribution as a density function at a certain degree of hydration. The proposed model is verified with the results of MIP tests.

3) Time-dependent moisture loss and shrinkage strain in early age concrete is obtained by integrating the multi-component hydration heat model, the micropore structure formation model and the moisture transport model into a finite element program. The applicability of the FE program is verified through comparison with experimental data.

4) A compressive strength development model which can consider the effects of temperature, age and porosity of early-age concrete is proposed. A stiffness development model which considers the interfacial transition zone and the effects of aggregate size and aggregate grading is also proposed based on micromechanics theory. These are verified through comparisons with experimental data.

5) The effects of chloride ions of sea sand used in concrete on the behavior of early-age concrete are investigated by experiment and are discussed. It is found that

these chloride ions increase shrinkage deformation but do not change hydration heat characteristics. A modification of shrinkage strain which considers the effects of chloride ions is carried out, and then verified through comparison with experimental data.

6) The cracking resistance of concrete wall structure at an early age is carried out by a finite element analysis which unifies the aforementioned proposed models. The analysis scheme used in this study may be used to evaluate the cracking resistance of early-age concrete effectively.

REFERENCES

[1] Maekawa, K., Chaube, R. and Kishi, T., 'Modeling of concrete performance: hydration, microstructure formation and mass transport', (Routledge, London and New York, 1999).

[2] van Breugel, K., 'Simulation of hydration and formation of structure in hardening cement-based materials', Ph.D. thesis, Delft Technological Institute (1991).

[3] de Borst, R. and van den Boogaard, A. H., 'Finite-element modeling of deformation and cracking in early-age concrete', *Journal of Engineering Mechanics* **120** (12) (1994) 2518-2534.

[4] Kishi, T. and Maekawa, K., 'Hydration heat model for blended cement including blast slag and fly ash', *Proceedings of the JCI* **15** (1) (1993) 1211-1216.

[5] Chaube, R. P. and Maekawa, K., 'Coupled moisture transport, structure formation and hydration in cementitious materials', *Proceedings of the JCI* **17** (1) (1995) 639-644.

[6] Chaube, R. P., 'Simulation of moisture transport, hydration and microstructure formation in cementitious materials', Ph.D. thesis, The University of Tokyo, (1996).

[7] Shimomura, T. and Maekawa, K., 'Analysis of the drying shrinkage behavior of concrete using a micromechanical model based on the micropore structure of concrete', *Magazine of Concrete Research* **49** (1) (1997) 303-322.

[8] Setzer, M. T., 'A model of hardened cement paste for linking shrinkage and creep phenomena', in 'Fundamental Research on Creep and Shrinkage of Concrete' (Martinus Nijhoff Publishers, 1982).

[9] Rastrup, E., 'Heat of hydration in concrete', *Magazine of Concrete Research* **6** (17) (1954) 79-92.

[10] Chanvillard, G. and D'Aloia, L., 'Concrete strength estimation at early ages: modification of the method of equivalent age', *ACI Materials Journal* **94** (6) (1997) 520-530.

[11] Monteiro, P. J. M., Maso, J. C. and Ollivier, J. P., 'The aggregate-mortar interface', *Cement and Concrete Research* **15** (1985) 953-958.

[12] Byun, K. J., Song, H. W. and Cho, H. J., 'Micromechanical-based evaluation of elastic moduli of concrete considering composite material behavior', in 'Structural Engineers World Congress '98 Conference Proceedings on CD-ROM', San Francisco, Calif. U.S.A., (1998), Paper Reference: T183-1.

[13] Nemat-Nasser, S. and Hori, M., 'Micromechanics: overall properties of heterogeneous materials', (North-Holland, Netherlands, 1993).

[14] Li, G., Zhao, Y. and Pang, S.-S., 'Four-phase sphere modeling of effective bulk modulus of concrete', *Cement and Concrete Research* **29** (1999) 839-845.

[15] Kim, J.-K., Moon, Y.-H. and Eo, S.-H., 'Compressive strength development of concrete with different curing time and temperature', *Cement and Concrete Research* **28** (12) (1998) 1761-1773.

[16] Brown, P. W., Harner, C. L. and Prosen, E. J., 'The effect of inorganic salts on tricalcium silicate hydration', *Cement and Concrete Research* **16** (1) (1986) 17-23.